Electronic Supplementary Material (ESI) for Environmental Science: Nano.

Supporting Information

2D-rGO-supported FePc bifunctional nanozyme with enhanced catalytic activity for thiosulfate detection and rhodamine B degradation

Feijin Zhou,[a] Wenying Cui,[a] Chenggang Liu,[a] Cheng Yao[a] and Chan Song*[a]

School of Chemistry and Molecular Engineering, Nanjing Tech University, Nanjing 211816, China.

Email: songchan@njtech.edu.cn

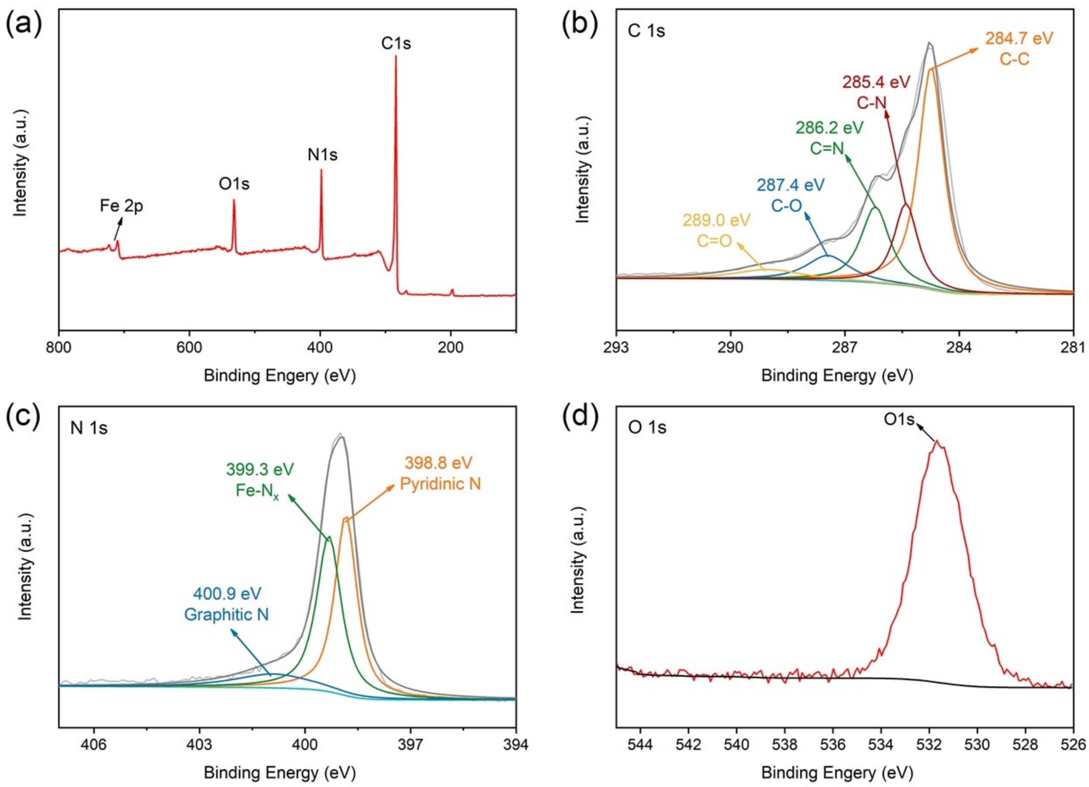

Fig. S1. High-resolution XPS spectra of XPS full spectra (a), C 1s spectra (b), N 1s spectra (c) and O 1s spectra (d) of FePc@rGO.

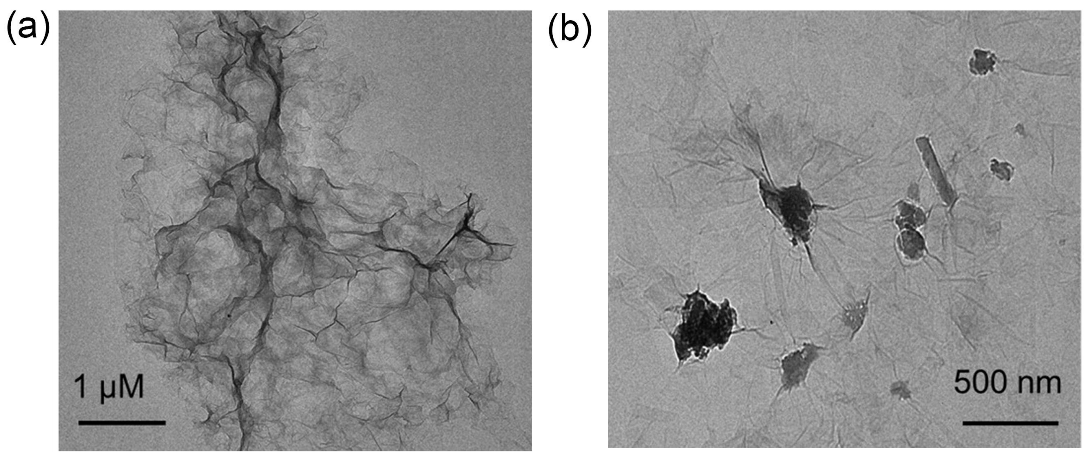

Fig. S2. TEM images of rGO (a) and FePc@rGO (b).

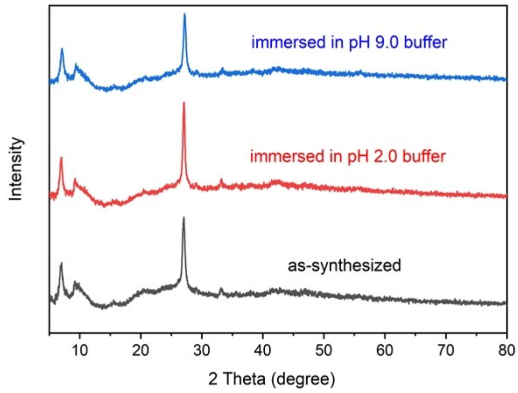

Fig. S3. XRD patterns of synthesized FePc@rGO and FePc@rGO immersed in different pH for 30 min.

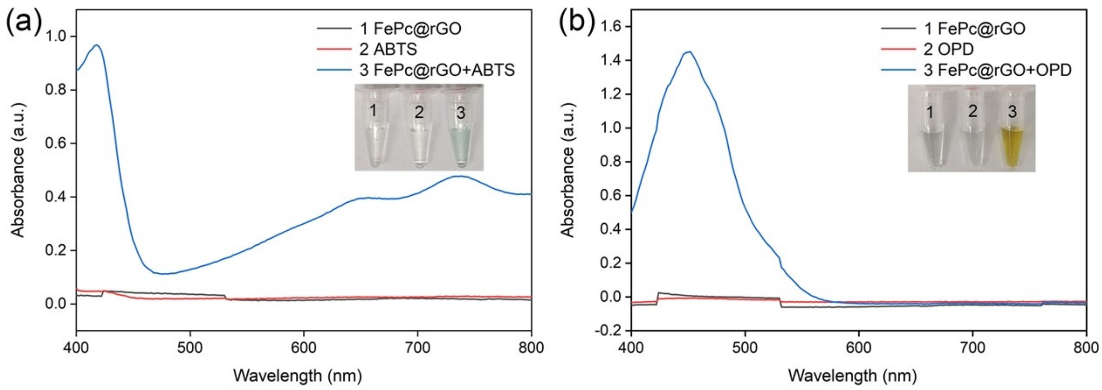

Fig. S4. The oxidation of ABTS (a) and OPD by using FePc@rGO as oxidase-like nanozymes.

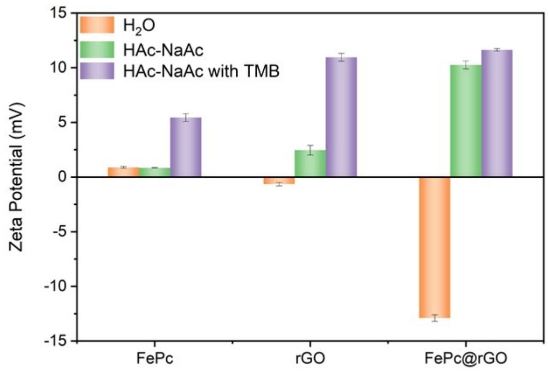

Fig. S5. Zeta potential of materials in water and zeta potential of materials in HAc-NaAc buffer (10 mM, pH 3.0) without and with the presence of TMB, respectively.

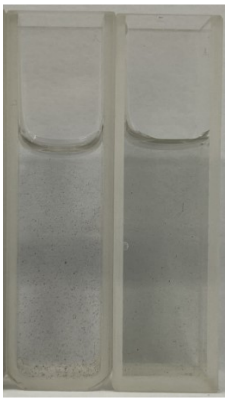

Fig. S6. The dispersion of FePc (left), and FePc@rGO (right) in water.

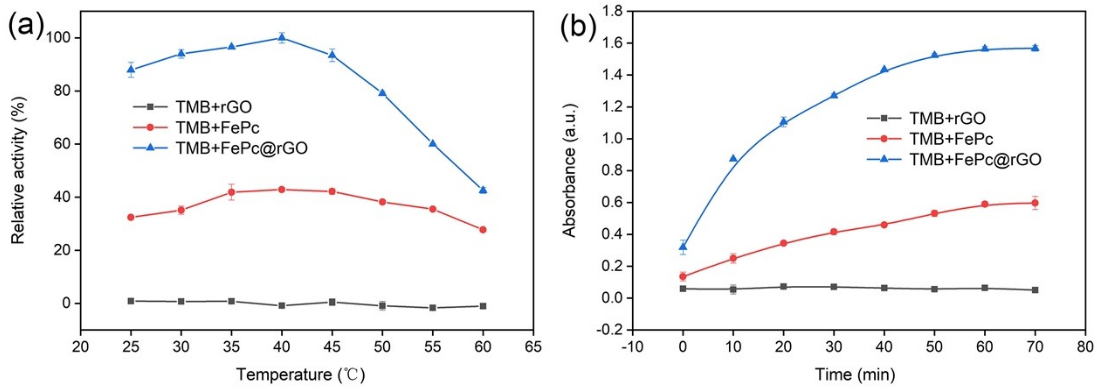

Fig. S7. (a) Effect of temperature on the oxidase-like activity of rGO, FePc and FePc@rGO. (b) The absorbance of TMB with different materials (rGO, FePc and FePc@rGO) at 652 nm vs time cures.

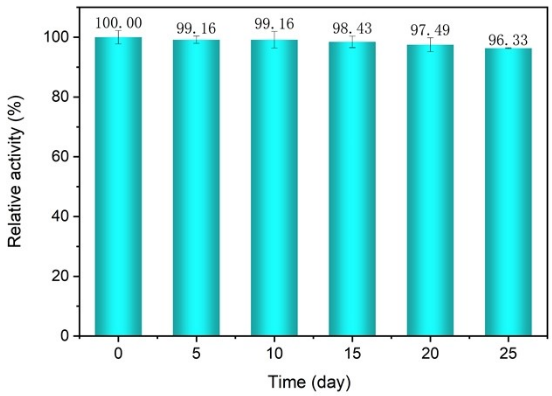

Fig. S8. Stability of the catalytic property provided by FePc@rGO.

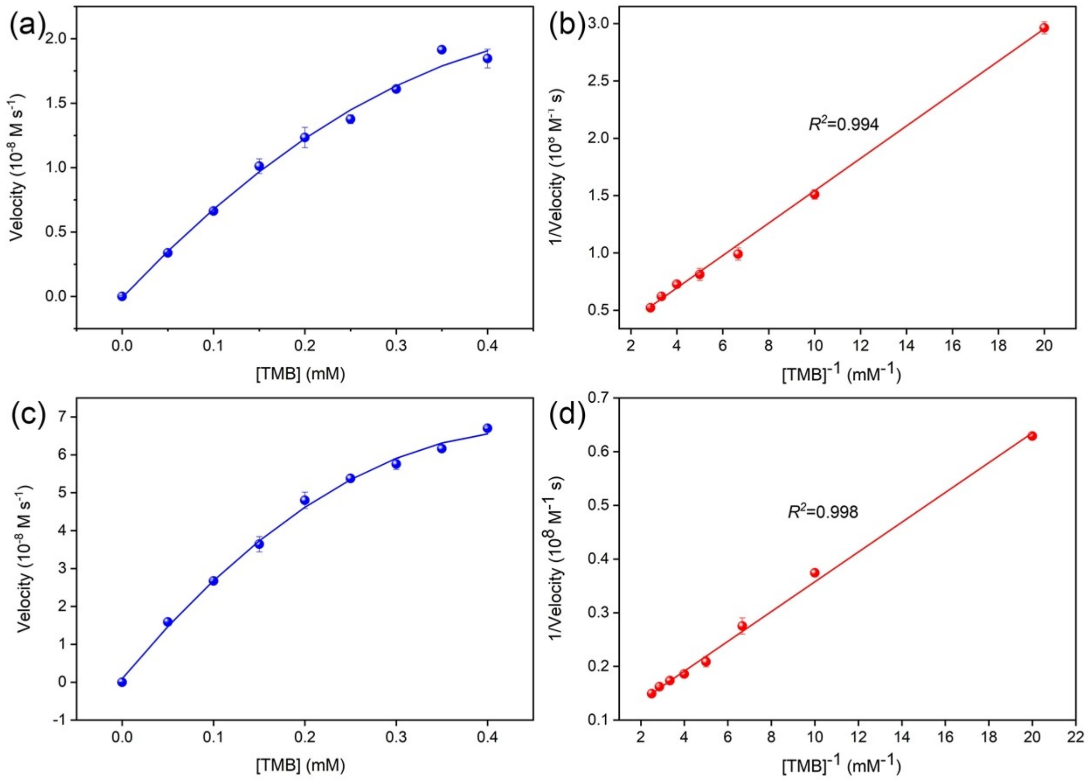

Fig. S9. Steady-state kinetic analyses of FePc and FePc@rGO using the Michaelis-Menten model (a and c) and the Lineweaver-Burk double inverse model (b and d). Plots of reaction rates at different TMB dosages (a and c). Double inverse plots of FePc and FePc@rGO with varying TMB concentration (b and d).

Table S1. The Michaelis–Menten constant (K_m) of FePc@rGO and other nanomaterials-based oxidase-like nanozymes to TMB.

Catalysts	K_m (mM)	V_{max} (10^{-8} M S^{-1})	Reference
Pt NPs	0.62	1.10	[1]
Pd cubes	0.43	1.80	[2]
Fe-N-C SAzymes	1.81	0.06	[3]
Cu_3/ND@G	2.89	11.50	[4]
NSC/$Co_6Ni_3S_8$	0.51	7.78	[5]
Au-PtNCs-GMP	2.42	5.20	[6]
FePc	**1.09**	**7.71**	**This work**
FePc@rGO	**0.35**	**12.45**	**This work**

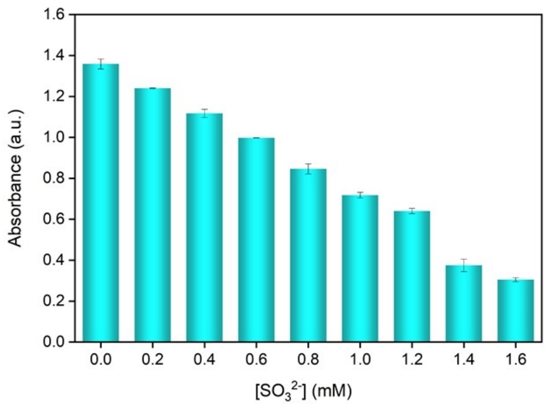

Fig. S10. The effect of sulfite on the oxidase-like catalytic activity of FePc@rGO.

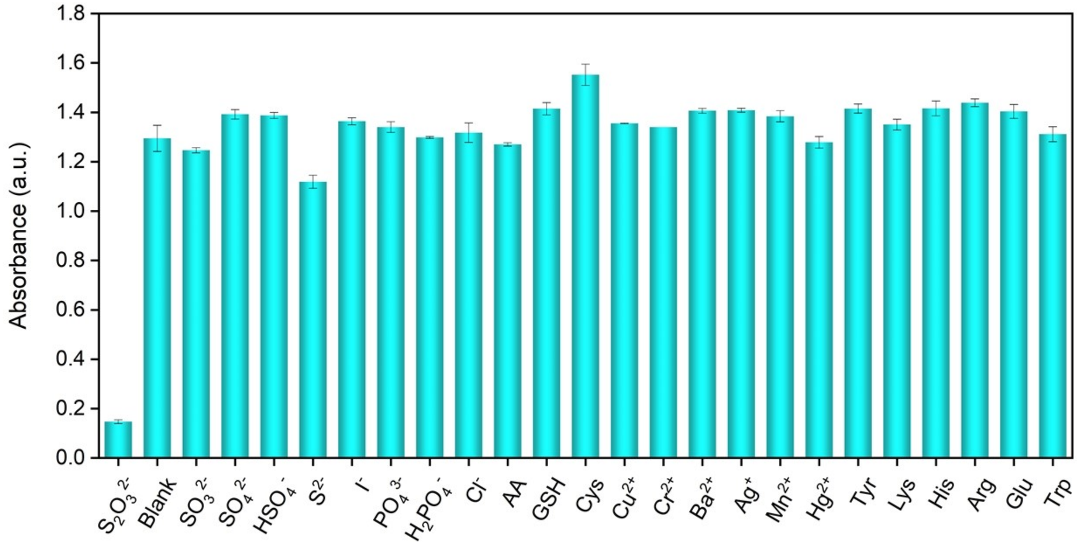

Fig. S11. The selectivity of the sensing platform for the detection of $S_2O_3^{2-}$. The concentration of each substance was 0.1 mM.

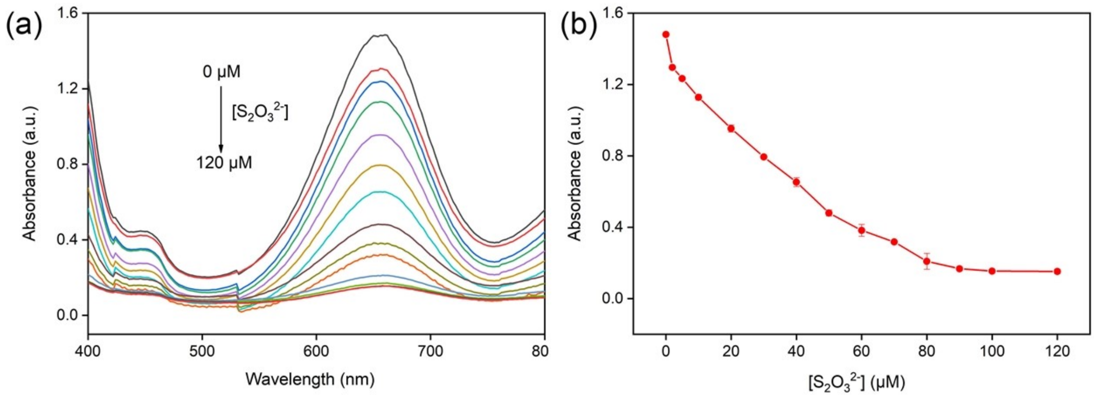

Fig. S12. (a) The UV-vis absorption spectra of FePc@rGO/TMB system with different concentration of $S_2O_3^{2-}$. (b) The absorption intensity of the $S_2O_3^{2-}$ sensing system at 652 nm.

Table S2. Comparison of different nanomaterials-based methods for the detection of $S_2O_3^{2-}$.

Materials	Methods	Detection limit (μM)	Linear range (μM)	Reference
Cu^{2+}-*p*-CPIP	Fluorometric	0.44	0.25-2.5	[7]
ASC	Fluorometric	0.149	0-26.0	[8]
TPA-T-Py	Fluorometric	0.97	1.0-5.0	[9]
Heme/SPE	Electrochemical	0.33	1.0-100	[10]
Ag NPs	Colorimetry	0.20	0.2-2.0	[11]
FePc@rGO	Colorimetry	**0.124**	**2.0-50.0**	**This work**

Table S3. Recoveries of thiosulfate in water samples.

Samples	Added (μM)	Recovered (μM)			Recovery (%)	RSD (%)
Tap water	5	5.42	5.25	4.84	103.4	5.77
	30	30.68	30.04	30.45	101.3	1.07
	50	48.93	48.58	48.46	97.3	0.50
Mineral water	5	4.89	4.95	5.25	100.6	3.83
	30	29.92	30.51	31.39	102.0	2.42
	50	48.35	48.35	49.16	97.2	0.96

Table S4. Comparison of RhB degradation by different catalysts.

Materials	pH	Catalyst (mg/L)	Time (min)	*k* (min^{-1})	Reference
$Co_3O_4/CoFe_2O_4$ HNCs	6-8	30	40	0.2451	[12]
C−CoCu−HNCs	4-9	20	60	0.2565	[13]
$CuBi_2O_4$	3.5-9.1	800	180	0.0179	[14]
Co (II)-doped TiO_2	3-9	500	30	0.248	[15]
porous Fe_2O_3	5-7	1500	60	0.0897	[16]
$CuFe_2O_4$–VO_x	5-8	100	16	0.2045	[17]
FePc@rGO	**3-10**	**10.0**	**10**	**0.3572**	**This work**

Reference

1 J. Liu, L. Meng, Z. Fei, P. J. Dyson and L. Zhang, On the origin of the synergy between the Pt nanoparticles and MnO_2 nanosheets in wonton-like 3D nanozyme oxidase mimics, *Biosens. Bioelectron*, 2018, **121**, 159-165.

2 T. Cai, G. Fang, X. Tian, J.-J. Yin, C. Chen and C. Ge, Optimization of antibacterial efficacy of noble-metal-based core-shell nanostructures and effect of natural organic matter, *ACS Nano*, 2019, **13**, 12694-12702.

3 Y. Wu, L. Jiao, X. Luo, W. Xu, X. Wei, H. Wang, H. Yan, W. Gu, B. Z. Xu, D. Du, Y. Lin and C. Zhu, Oxidase-like Fe-N-C single-atom nanozymes for the detection of acetylcholinesterase activity, *Small*, 2019, **15**, 1903108.

4 F. Meng, M. Peng, Y. Chen, X. Cai, F. Huang, L. Yang, X. Liu, T. Li, X. Wen, N. Wang, D. Xiao, H. Jiang, L. Xia, H. Liu and D. Ma, Defect-rich graphene stabilized atomically dispersed Cu_3 clusters with enhanced oxidase-like activity for antibacterial applications, *Applied Catalysis B: Environmental*, 2022, **301**, 120826.

5 T. Liu, Y. Li, J. Gu, L. Zhang, F. Qian, B. Li and X. Wang, Achieving smartphone-based colorimetric assay for Hg^{2+} with a bimetallic site strategy based on Hg^{2+}-triggered oxidase-like catalytic activity of NSC/$Co_6Ni_3S_8$ nanocomposite, *Anal. Chim. Acta*, 2023, **1278**, 341734.

6 C.-X. Zhang, Y.-C. Gao, H.-W. Li and Y. Wu, Gold-platinum bimetallic nanoclusters for oxidase-like catalysis, *ACS Appl. Nano Mater.*, 2020, **3**, 9318-9328.

7 Q. Wang, H. Sun, W. Sha, J. Chen, L. Gu, D. Wang and X. Tang, An optical material for the detection of trace $S_2O_3^{2-}$ in milk based on a copper complex, *Biometals*, 2017, **30**, 441-447.

8 Y.-H. Deng, R.-Y. Li, J.-Q. Zhang, Y.-F. Wang, J.-T. Li, W.-T. Guo and W.-K. Dong, A novel turn-on fluorogenic aldehyde-appended salamo-like copper (II) complex probe for the simultaneous detection of $S_2O_3^{2-}$ and GSH, *New J. Chem.*, 2021, **45**, 8597-8607.

9 J. Li, H. Huang, C. Zhang, X. Chen, Y. Hu and X. Huang, Dual-key-and-lock AIE probe for thiosulfate and Ag^+ detection in mitochondria, *Talanta*, 2023, **255**, 124222.

10 G.-C. Han, H. Li, A. Ferranco, Tao Zhan, Y. Cheng, Z. Chen, M. Xue, X.-Z. Feng and H.-B. Kraatz, The construction of a simple sensor for the simultaneous detection of nitrite and thiosulfate by heme catalysis, *RSC Adv.*, 2020, **10**, 35007–35016.

11 C. Dong, Z. Wang, Y. Zhang, X. Ma, M. Z. Iqbal, L. Miao, Z. Zhou, Z. Shen and A. Wu,

High-performance colorimetric detection of thiosulfate by using silver nanoparticles for smartphone-based analysis, *ACS Sens.*, 2017, **2**, 1152–1159.

12 S. Jiang, G. Su, J. Wu, C. Song, Z. Lu, C. Wu, Y. Wang, P. Wang, M. He, Y. Zhao, Y. Jiang, X. Zhao, H. Rao and M. Sun, $Co_3O_4/CoFe_2O_4$ hollow nanocube multifunctional nanozyme with oxygen vacancies for deep-learning-assisted smartphone biosensing and organic pollutant degradation, *ACS Appl. Mater. Interfaces*, 2023, **15**, 11787–11801.

13 S. Li, Y. Hou, Q. Chen, X. Zhang, H. Cao and Y. Huang, Promoting active sites in MOF-derived homobimetallic hollow nanocages as a high-performance multifunctional nanozyme catalyst for biosensing and organic pollutant degradation, *ACS Appl. Mater. Interfaces*, 2020, **12**, 2581–2590.

14 Y. Wang, F. Li, T. Xue, C. Liu, D. Yuan, F. Qi and B. Xu, Heterogeneous activation of peroxymonosulfate by hierarchical $CuBi_2O_4$ to generate reactive oxygen species for refractory organic compounds degradation: morphology and surface chemistry derived reaction and its mechanism, *Environ Sci Pollut Res*, 2018, **25**, 4419–4434.

15 H. Wang, Q. Gao, H. Li, B. Han, K. Xia and C. Zhou, One-pot synthesis of a novel hierarchical Co (II)-doped TiO_2 nanostructure: toward highly active and durable catalyst of peroxymonosulfate activation for degradation of antibiotics and other organic pollutants, *Chem. Eng. J.*, 2019, **368**, 377–389.

16 F. Ji, C. Li, X. Wei and J. Yu, Efficient performance of porous Fe_2O_3 in heterogeneous activation of peroxymonosulfate for decolorization of Rhodamine B, *Chem. Eng. J.*, 2013, **231**, 434–440.

17 R. Salami, M. Amini, M. Bagherzadeh and K. H. Chae, Vanadium oxide-supported copper ferrite nanoparticles: a reusable and highly efficient catalyst for rhodamine B degradation via activation of peroxymonosulfate, *Appl Organomet Chem.*, 2021, 35, e6367.